Nuclear Medicine and Biology 100–101 (2021) 44–51

Contents lists available at ScienceDirect

Nuclear Medicine and Biology

journal homepage: www.elsevier.com/locate/nucmedbio

BLZ945 derivatives for PET imaging of colony stimulating factor-1 receptors in the brain☆

Berend van der Wildt [a,b], Zheng Miao [a], Samantha T. Reyes [a], Jun H. Park [a], Jessica L. Klockow [a], Ning Zhao [a], Alex Romero [a], Scarlett G. Guo [a], Bin Shen [a], Albert D. Windhorst [b], Frederick T. Chin [a,*]

[a] Molecular Imaging Program at Stanford (MIPS), Department of Radiology, Stanford University, School of Medicine, Stanford, CA, USA
[b] Amsterdam UMC, Vrije Universiteit Amsterdam, Radiology & Nuclear Medicine, de Boelelaan 1117, Amsterdam, Netherlands

ARTICLE INFO

Article history:
Received 16 March 2021
Received in revised form 4 May 2021
Accepted 17 June 2021

Keywords:
Positron emission tomography
Colony stimulating Factor-1 receptor
Tumor associated macrophages
Glioblastoma
Companion diagnostic
BLZ945

ABSTRACT

Background: The kinase colony stimulating factor-1 receptor (CSF-1R) has recently been identified as a novel therapeutic target for decreasing tumor associated macrophages and microglia load in cancer treatment. In glioblastoma multiforme (GBM), a high-grade cancer in the brain with extremely poor prognosis, macrophages and microglia can make up to 50% of the total tumor mass. Currently, no non-invasive methods are available for measuring CSF-1R expression *in vivo*. The aim of this work is to develop a PET tracer for imaging of CSF-1R receptor expression in the brain for future GBM patient selection and treatment monitoring.
Methods: **BLZ945** and a derivative that potentially allows for fluorine-18 labeling were synthesized and evaluated *in vitro* to determine their affinity towards CSF-1R. **BLZ945** was radiolabeled with carbon-11 by *N*-methylation of *des-methyl*-**BLZ945** using [^{11}C]CH_3I. Following administration to healthy mice, metabolic stability of [^{11}C]**BLZ945** in blood and brain and activity distribution were determined *ex vivo*. PET scanning was performed at baseline, efflux transporter blocking, and CSF-1R blocking conditions. Finally, [^{11}C]**BLZ945** binding was evaluated *in vitro* by autoradiography on mouse brain sections.
Results: **BLZ945** was the most potent compound in our series with an IC_{50} value of 6.9 ± 1.4 nM. **BLZ945** was radiolabeled with carbon-11 in 20.7 ± 1.1% decay corrected radiochemical yield in a 60 min synthesis procedure with a radiochemical purity of >95% and a molar activity of 153 ± 34 GBq·μmol^{-1}. *Ex vivo* biodistribution showed moderate brain uptake and slow wash-out, in addition to slow blood clearance. The stability of **BLZ945** in blood plasma and brain was >99% at 60 min post injection. PET scanning demonstrated **BLZ945** to be a substrate for efflux transporters. High brain uptake was observed, which was shown to be mostly non-specific. In accordance, *in vitro* autoradiography on brain sections revealed high non-specific binding.
Conclusions: [^{11}C]**BLZ945**, a CSF-1R PET tracer, was synthesized in high yield and purity. The tracer has high potency for the target, however, future studies are warranted to address non-specific binding and tracer efflux before **BLZ945** or derivatives could be translated into humans for brain imaging.

1. Introduction

Glioblastoma multiforme (GBM) is a grade IV brain cancer with extremely poor prognosis; chemotherapy alone or combined with radiation therapy and surgery only prolongs the median survival time of GBM patients from 10 months to 14 months [1–3]. Newer therapies, such as bevacizumab, approved as a second line treatment for patients with recurrent GBM, and local drug-release implants introduced after surgical resection, only provide limited effects [4–6]. Therefore, novel treatment strategies are essential for combatting this devastating disease.

A new strategic target for GBM treatment is the colony stimulating factor 1 receptor (CSF-1R), which is expressed on tumor-associated microglia and macrophages (TAMs). Together TAMs can comprise up to 50% of the tumor mass [7,8]. Microglia and macrophages depend on the activation of CSF-1R by their endogenous ligand Colony Stimulating Factor-1 (CSF-1) for their survival and proliferation. In the absence of CSF-1 or the presence of CSF-1R inhibitors macrophage and microglia are unable to differentiate and will eventually be depleted from the tissue. This strategy of CSF-1R inhibition has resulted in reduced GBM tumor mass and a corresponding prolonged survival in GBM mouse models and thus provides a promising new approach to combatting brain cancers [9]. Currently, many small molecule and antibody inhibitors of CSF-1R are in (pre)clinical development [10,11]. In addition to cancer, CSF-1R has been implicated as a pharmacological target for neuroinflammatory and neurodegenerative diseases [12].

☆ Given his role as Editor in Chief of this journal, Albert D. Windhorst had no involvement in the peer-review of this article.

* Corresponding author at: 3165 Porter Drive, CA, 94304 Palo Alto, USA.
E-mail address: chinf@stanford.edu (F.T. Chin).

https://doi.org/10.1016/j.nucmedbio.2021.06.005
0969-8051/

Positron emission tomography (PET) is a molecular imaging technique that allows for the quantitative and non-invasive assessment of biological processes such as transporter and enzyme activity and receptor density [13]. A validated CSF-1R selective PET tracer would have enormous value in facilitating study of brain diseases, selecting appropriate patient therapies, monitoring treatment responses, and developing new drugs. Three CSF-1R PET tracers have been reported to date (Fig. 1) [14–16]. However, these tracers suffer from various limitations, which could prevent their clinical translation. *E.g.* [^{18}F]**10** has poor affinity and low selectivity [14], whereas [^{11}C]**AZD6495** displayed insufficient brain uptake [15]. The most promising CSF-1R tracer reported to date is [^{11}C]**CPPC**, which has a high affinity for CSF-1R and displays good brain penetration in mice and baboon [16]. However, this compound is derived from a rather non-selective compound [17] and in addition, shows high non-specific binding in the brain.

Among the multiple CSF-1R small molecule inhibitors currently in clinical development [17–22] is **BLZ945**, a highly potent and selective CSF-1R inhibitor (K_i = 1 nM, > 3200 fold selectivity over other kinases) [9]. This CSF-1R inhibitor demonstrated great efficacy in GBM mice, implicating good brain uptake. Taken together, **BLZ945** has high potential for translation into the first highly potent and selective CSF-1R PET tracer, either by direct labeling with carbon-11 or by development of analogues that allow for fluorine-18 labeling. The aim of the current study is to develop a new CSF-1R PET tracer based on **BLZ945** as a companion diagnostic for imaging CSF-1R expression in the brain.

2. Material and methods

2.1. General

All chemical reagents and solvents were obtained from commercial suppliers and used as received. Microwave reactions were performed on a CEM Discover Legacy (Matthews, NC, USA). Reaction monitoring was performed by thin layer chromatography on pre-coated silica 60 F254 aluminum plates (Merck, Darmstadt, Germany). Spots were visualized with UV light (254 nm), $KMnO_4$, or ninhydrin staining. NMR spectroscopy was performed using an Agilent 400 MR (Agilent Technologies, Santa Clara, CA, USA) with chemical shifts (δ) reported in parts per million (ppm) relative to the solvent ($CDCl_3$ ^{1}H: 7.26 ppm, ^{13}C: 77.16 ppm; DMSO-d_6 ^{1}H: 2.50 ppm, ^{13}C 39.52 ppm; CD_3OD ^{1}H: 3.31 ppm, ^{13}C: 49.00 ppm). High resolution mass spectrometry was performed on a Bruker Daltonics - apex-Qe (Bruker, Billerica, MA, USA) in either positive or negative ion mode. Enzyme inhibition assay kits (*Z*-LYTE™ assay) and human recombinant enzymes were obtained from ThermoFisher Scientific (Waltham, MA, USA). Fluorescent readout of 384-well plates was performed on a fluorimeter (Safire, Tecan, XFluo). Carbon-11 was prepared by the ^{14}N(p,α)^{11}C nuclear reaction on a GE PETtrace 880 cyclotron and was delivered as [^{11}C]CO_2 using nitrogen as a carrier gas to the experimental set up (GE TRACERlab FX-C Pro, Boston, MA, USA). Preparative HPLC was performed on a Dionex P680 HPLC pump equipped with a Phenomenex Gemini semi preparative HPLC column (250 × 10 mm, 5u) using a mixture of A) H_2O and B) MeCN according to the following scheme (Method A): 0 min, 35% B; 2 min, 35% B; 20 min, 60% B. UV detection was performed using a Knauer k-2001 UV detector. Radioactivity levels were determined using a dose calibrator (Capintec CRC-15 PET). Analytical HPLC was performed on an Agilent Technologies 1200 HPLC system (Agilent Technologies, Santa Clara, CA, USA) connected to a Raytest GABI* radiodetector (Elisia Raytest GmbH, Straubenhardt, Germany, sensitivity 370 Bq (10 nCi)) using a Luna 5u C18 column (250 × 4.6 mm, 5 μm particle size) using a mixture of A) H_2O and B) MeCN as a mobile phase according to the following scheme (Method B): 0 min, 50% B; 15 min, 70% B; 15.1 min, 95% B; 17 min, 95% B; 17.1 min, 50% B; 17.1–20.0 min 50% B. Mice were housed in 12 h light/dark cycles and were provided food and water *ad libitum*. Blood was obtained by arterial puncture and centrifuged using an ultracentrifuge system (Eppendorf Minispin Plus). Gamma counting was performed on a Hidex Automatic Gamma Counter (Turku, Finland). TLC plates were exposed to a phosphorimager screen (Fujifilm, Valhalla, NY, USA) for 30 min in a cassette (Hypercasette, Amersham Biosciences, Little Chalfont, United Kingdom) and subsequently developed using a Typhoon Trio Imager (GE Healthcare, Waukesha, WI, USA). Images were analyzed using ImageJ version 1.49v (National Institute of Health, USA). PET scanning was performed on a Siemens Inveon dPET and Siemens Inveon Hybrid MicroPET/CT (Munich, Germany) with identical PET components. Scans were acquired in list mode and rebinned into the following frame sequence: 7.5 s, 4 × 15 s, 37.5 s, 3 × 60 s, 180 s, 9 × 300 s and 435 s. Following a transmission scan for attenuating correction, reconstruction was performed (3D OSEM). Images were analyzed using PMOD (PMOD Technologies LLC, Zurich, Switzerland) by drawing regions of interest over selected organs and tissues. PLX3397 was purchased from Selleckchem. CPPC and 'compound 22' were synthesized using reported literature procedures [16,23]. Spectroscopic and spectrometric data (^{1}H NMR, ^{13}C NMR and ESI-HRMS) was in accordance with reported values (data not shown).

2.2. Chemistry

Compound 1 ((1*R*,2*R*)-2-((6-methoxybenzo[*d*]thiazol-2-yl)amino) cyclohexan-1-ol):

A solution of 2-chloro-6-methoxybenzo[*d*]thiazole (1.0 g, 5.0 mmol), (1*R*,2*R*)-2-aminocyclohexan-1-ol (0.76 g, 5.0 mmol), TEA (1.7 mL, 12.5 mmol) in NMP (2 mL) was heated at 120 °C for 48 h. The reaction mixture was cooled to rt. and the precipitates were removed by filtration. The filtrate was concentrated *in vacuo* and purified by flash column chromatography (EtOAc/hexanes 1:1) to afford the product as a white solid (0.82 g, 59%). ^{1}H NMR (400 MHz, $CDCl_3$): δ = 7.39 (d, 1H, J = 9.1 Hz), 7.05 (d, 1H, J = 2.5 Hz), 6.86 (dd, 1H, J = 2.6, 8.8 Hz), 5.81 (bs, 1H), 3.79 (s, 3H), 3.44 (m, 2H), 2.11 (m, 2H), 1.70 (m, 2H), 1.41–1.16 (m, 4H), 0.27 (s, 1H). ^{13}C NMR (101 MHz, $CDCl_3$): δ = 166.81, 155.35, 145.93, 131.43, 119.21, 113.58, 105.47, 75.28, 61.81, 55.99, 34.27, 32.07, 24.86, 24.15. ESI-HRMS: m/z calculated for $C_{14}H_{18}N_2O_2S$: 278.1089; found: 301.0980 $[M + Na]^+$.

Compound 2 (2-(((1*S*,2*R*)-2-hydroxycyclohexyl)amino)benzo[*d*] thiazol-6-ol).

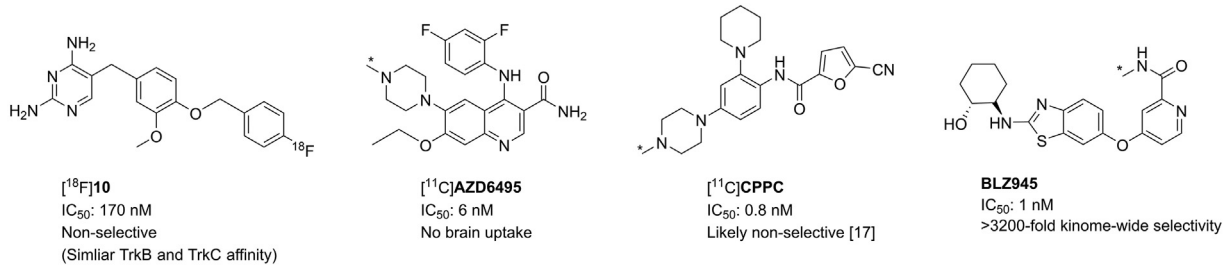

Fig. 1. Previously reported CSF-1R PET tracers [14–16] and **BLZ945** as a potential PET tracer with improved characteristics (this work). The positions of the carbon-11 labels are depicted with *.

To a solution of **1** (0.56 g, 2.0 mmol) and TEA (0.56 mL, 4.0 mmol) in DCM (5 mL) at 0 °C was added boron tribromide (1.0 M in DCM, 4.0 mL, 4.0 mmol) and the resulting solution was stirred for 3 h while allowing gradual warming to room temperature. After concentration *in vacuo* the residue was purified by flash column chromatography (EtOAc/hexanes 2:1) to afford the product as a white solid (0.48 g, 90%). ^{1}H NMR (400 MHz, CD_3OD): $\delta = 7.22$ (d, 1H, $J = 8.7$ Hz), 6.99 (d, 1H, $J = 2.1$ Hz), 6.73 (dd, 1H, $J = 2.2$, 8.6 Hz), 3.52 (m, 1H), 3.42 (m, 1H), 2.17 (m, 1H), 2.01 (m, 1H), 1.73 (m, 2H), 1.41–1.21 (m, 4H). ^{13}C NMR (101 MHz, CD_3OD): $\delta = 167.59$, 153.70, 146.27, 132.03, 119.09, 114.91, 107.85, 74.50, 61.49, 35.38, 32.59, 25.60, 25.27. ESI-HRMS: *m/z* calculated for $C_{13}H_{16}N_2O_2S$: 264.0932; found: 265.1006 $[M + H]^+$.

Compound 3 (4-((2-(((1*S*,2*R*)-2-hydroxycyclohexyl)amino)benzo[*d*]thiazol-6-yl)oxy)picolinamide):

A mixture of **2** (66 mg, 0.25 mmol), methyl 4-fluoropicolinate (39 mg, 0.25 mmol) and K_2CO_3 (69 mg, 0.50 mmol) in DMF (4 mL) was heated at 100 °C for 16 h. The mixture was diluted with EtOAc, filtered and concentrated *in vacuo*. After flash column chromatography (EA -> 2% MeOH in EtOAc) the product was obtained as a yellow solid (51 mg, 51%). ^{1}H NMR (400 MHz, $CDCl_3$): $\delta = 8.54$ (d, 1H, $J = 5.6$ Hz), 7.62 (d, 1H, $J = 2.5$ Hz), 7.52 (d, 1H, $J = 8.6$ Hz), 7.28 (d, 1H, $J = 2.4$ Hz), 7.00 (dd, 1H, $J = 2.5$, 8.7 Hz), 6.97 (dd, 1H, $J = 2.5$, 5.6 Hz), 5.9 (m, 2H), 3.96 (s, 3H), 3.51 (m, 2H), 2.18 (m, 2H), 1.74 (m, 2H), 1.33 (m, 4H). ^{13}C NMR (101 MHz, $CDCl_3$): $\delta = 168.37$, 166.55, 165.53, 151.41, 149.97, 148.21, 131.94, 119.87, 119.37, 114.73, 113.51, 113.39, 113.38, 75.24, 61.88, 53.13, 34.35, 32.02, 24.81, 24.15. ESI-HRMS: *m/z* calculated for $C_{20}H_{21}N_3O_4S$: 399.1253; found: 422.1145 $[M + Na]^+$.

Compound 4 4-((2-(((1*S*,2*R*)-2-hydroxycyclohexyl)amino)benzo[*d*]thiazol-6-yl)oxy)picolinamide.

A mixture of **2** (66 mg, 0.25 mmol), 4-fluoropicolinamide (35 mg, 0.25 mmol) and K_2CO_3 (69 mg, 0.50 mmol) in DMF (4 mL) was heated at 100 °C for 16 h. The mixture was diluted with EtOAc, filtered and concentrated *in vacuo*. After flash column chromatography (EA -> 2% MeOH in EA) the product was obtained as a yellow solid (80 mg, 80%). ^{1}H NMR (400 MHz, $CDCl_3$): $\delta = 8.38$ (d, 1H, $J = 5.6$ Hz), 7.86 (d, 1H, $J = 4.2$ Hz), 7.67 (d, 1H, $J = 2.6$ Hz), 7.48 (d, 1H, $J = 8.7$ Hz), 7.27 (m, 1H), 6.97 (m, 2H), 6.24 (bs, 1H), 6.07 (d, 1H, $J = 4.1$ Hz), 4.32 (bs, 2H), 3.49 (m, 2H), 2.17 (m, 2H), 1.73 (m, 2H), 1.43–1.23 (m, 4H). ^{13}C NMR (101 MHz, $CDCl_3$): $\delta = 168.42$, 166.92, 166.62, 151.81, 150.02, 149.98, 148.17, 131.86, 119.67, 119.32, 114.43, 113.52, 110.41, 74.93, 61.90, 34.28, 31.92, 24.79, 24.19. ESI-HRMS: *m/z* calculated for $C_{19}H_{20}N_4O_3S$: 384.1256; found: 385.1331 $[M + H]^+$.

Compound 5 *N*-(2-fluoroethyl)-4-((2-(((1*S*,2*R*)-2-hydroxycyclohexyl)amino)benzo[*d*]thiazol-6-yl)oxy)picolinamide.

A solution of compound **3** (40 mg, 0.10 mmol) in MeOH/THF/KOH (4 M in H_2O) (1 mL, 4:9:2, v/v/v) was stirred at room temperature for 1 h. The solution was concentrated *in vacuo*, diluted with water (10 mL) and then acidified to pH 3 with 1 M HCl. The mixture was extracted with DCM (3 × 10 mL). The combined organic fractions were concentrated to dryness and the residue was resuspended in DMF (2 mL). Then, D*i*PEA (39 mg, 0.30 mmol), 2-fluoroethylamine·HCl (10 mg, 0.10 mmol) and HATU (45 mg, 0.10 mmol) were added and the solution was left for 16 h at room temperature. After concentration *in vacuo*, the residue was purified by flash column chromatography (2% MeOH in DCM) to afford the product as a white solid (25 mg, 58%). Intermediate: ^{1}H NMR (400 MHz, CD_3OD): $\delta = 8.62$ (d, 1H, $J = 6.1$ Hz), 7.75 (m, 2H), 7.64 (d, 1H, $J = 8.7$ Hz), 7.39 (m, 2H), 3.55 (m, 2H), 2.14 (m, 2H), 1.82 (m, 2H), 1.43 (m, 4H); ^{13}C NMR (101 MHz, CD_3OD): $\delta = 171.25$, 170.23, 163.84, 150.59, 149.69, 147.97, 140.89, 127.96, 121.88, 117.38, 116.50, 116.42, 114.62, 74.55, 63.97, 35.40, 31.83, 25.51, 25.10. Title compound **5**: ^{1}H NMR (400 MHz, CD_3OD): 8.46 (d, 1H, $J = 5.6$ Hz), 7.54 (s, 1H), 7.47 (d, 1H, $J = 8.6$ Hz), 7.41 (s, 1H), 7.04 (m, 2H), 4.61 (t, 1H, $J = 5.1$ Hz), 4.49 (t, 1H, $J = 5.1$ Hz), 3.66 (m, 3H), 3.46 (m, 1H), 2.20 (m, 1H), 2.06 (m, 1H), 1.78 (m, 2H), 1.37 (m, 4H); ^{13}C NMR (101 MHz, CD_3OD): 169.77, 168.46, 166.52, 153.01, 151.54, 151.45, 149.31, 132.83, 120.08, 119.70, 115.19, 114.69, 110.77, 83.08 (d, $J = 167.7$ Hz), 74.35, 61.66, 41.06 (d, $J = 21.3$ Hz), 35.44, 32.53, 25.62, 25.29.

4-((2-(((1*S*,2*R*)-2-hydroxycyclohexyl)amino)benzo[*d*]thiazol-6-yl)oxy)-*N*-methylpicolinamide, **BLZ945**:

To a solution of **3** (25 mg, 63 μmol) in THF was added methylamine·HCl (21 mg, 0.30 mmol) and K_2CO_3 (43 mg, 0.30 mmol). The mixture was reacted for 16 h at 50 °C. After filtration and concentration *in vacuo*, the product was purified by flash column chromatography (EA -> 2% MeOH in EA) to obtain the product as an off-white solid (20 mg, 80%). ^{1}H NMR (400 MHz, $CDCl_3$): $\delta = 8.35$ (d, 1H, $J = 5.6$ Hz), 8.02 (m, 1H), 7.68 (d, 1H, $J = 2.5$ Hz), 7.49 (d, 1H, $J = 8.7$ Hz), 7.27 (s, 1H), 6.99 (dd, 1H, $J = 2.5$, 8.7 Hz), 6.92 (dd, 1H, $J = 2.6$, 5.6 Hz), 6.18 (bs, 1H), 3.72 (bs, 1H), 3.50 (m, 2H), 3.00 (d, 3H, $J = 5.2$ Hz), 2.11 (m, 2H), 1.74 (m, 2H), 1.44–1.24 (m, 4H). ^{13}C NMR (101 MHz, $CDCl_3$): $\delta = 168.43$, 166.94, 164.75, 152.26, 149.82, 149.77, 148.27, 131.81, 119.65, 119.33, 114.02, 113.52, 110.15, 75.06, 61.88, 34.28, 31.93, 26.29, 24.79, 24.17. ESI-HRMS: *m/z* calculated for $C_{20}H_{22}N_4O_3S$: 398.1413; found: 421.1308 $[M + Na]^+$.

2.3. In vitro IC_{50} determination

Affinities for designed compounds were determined using a commercially available Z'-LYTE™ assay according to the manufacturer's instructions. Briefly, to a 384 well plate were added the respective kinase (either CSF-1R, PDGFR-β or c-KIT in a final concentration of 0.5, 1.0 and 1.0 ng/μL, respectively) in supplied kinase buffer, ATP (in a final concentration of 50 μM for CSF-1R and PDGFR-β, 100 μM for c-KIT), the respective inhibitor (2-fold dilution series in a concentration range from 1 μM to 0.5 nM), and the assay FRET-peptide. The resulting solutions (total volume of 10 μL per well) were incubated at room temperature for 1 h, followed by the addition of protease solution (5 μL per well). After careful mixing, the solutions were incubated for 1 h followed by the addition of stop buffer (5 μL per well). Readout of the plate was performed using excitation wavelength of 400 nm and emission wavelengths of 445 nm (coumarin) and 520 nm (fluorescein) with a 12 nm bandwidth. Negative control and positive control reactions were performed by omission of ATP and inhibitor, respectively. The obtained values are the result of three independent experiments and are expressed as average IC_{50} value ± standard deviation.

2.4. Radiosynthesis

After proton bombardment, $[^{11}C]CO_2$ was delivered to a TRACERlab FXC-pro module and trapped on a mixture of molecular sieves, precharged with hydrogen gas, and nickel. After completing delivery, the molecular sieve trap was heated to 350 °C and the formed $[^{11}C]CH_4$ was released to a silica trap, cooled to −80 °C using liquid nitrogen. This trap was heated to release $[^{11}C]CH_4$ into a closed circuit, where it was mixed with iodine vapor and converted to $[^{11}C]CH_3I$ at 720 °C. The $[^{11}C]CH_3I$ that was formed was accumulated on a cooled Porapak trap. When the radioactivity levels on this Porapak trap reached a plateau, it was heated to 220 °C to release $[^{11}C]CH_3I$, which was transferred to a reaction vial using a gentle stream of helium (20 mL/min). The reaction vial was previously charged with precursor **4** (1.0 mg, 2.6 μmol) and TBAOH (10 μL, 1.0 M in MeOH) in DMSO (400 μL) and was loaded with $[^{11}C]CH_3I$ until radioactivity reached a maximum. The reactor was sealed and the reaction solution was heated at 100 °C for 4 min and subsequently cooled to 20 °C. Next, the reaction solution was diluted with H_20 (1.0 mL) and purified using HPLC using method A. The collected HPLC product fraction was diluted with H_2O (40 mL) and passed over a preconditioned solid phase extraction cartridge (C_{18} Sep-Pak Light, Waters). After washing the cartridge with H_2O (10 mL), the product was obtained by sequential elution with ethanol (1.0 mL) and saline (9.0 mL). A sample was analyzed by analytical HPLC to determine the (radio)chemical purity and molar activity (Method B).

2.5. Partition coefficient LogD

The partitioning of [^{11}C]**BLZ945** between 1-octanol and 0.2 M phosphate buffer (pH = 7.4) was determined by vigorously mixing [^{11}C]BLZ945 (100 μL, 20 MBq) with a solution of 0.2 M phosphate buffer (2 mL, pH 7.4) and 1-octanol (2 mL) for 1 min using a vortex apparatus. After a settling period of 1 h, three samples of 100 μL were taken from both layers. Samples were counted for radioactivity and the Log D values were calculated according to the following formula: $\text{Log } D_{oct,7.4} = \text{Log } (A_{oct}/A_{\text{phosphate buffer}})$, where A_{oct} and $A_{\text{phosphate buffer}}$ represent average radioactivities of three 1-octanol and three phosphate buffer samples, respectively. The result is expressed as mean ± standard deviation ($n = 3$).

2.6. Plasma stability

[^{11}C]**BLZ945** (50 μL, 10 MBq) was added to freshly thawed (500 μL) mouse plasma (Sigma Aldrich, catalogue number P9275) and incubated at 37 °C for 1 h. Ice-cold acetonitrile (1.0 mL) was added and the mixture was centrifuged for 5 min at 15,000 RPM. An aliquot of the supernatant was analyzed by analytical HPLC using method B (retention time of [^{11}C]**BLZ945** is 8.4 min).

2.7. Radiometabolite analysis

Mice (10–16 weeks old, 25–30 g, n = 3 per time point) were injected with [^{11}C]**BLZ945** (100 μL, approximately 10 MBq) under isoflurane anesthesia (2% in O_2 at 1 L/min). At the indicated time-points, blood was collected by arterial puncture, approximately 0.5 mL) and transferred to a Heparin coated Eppendorf tube. Mice were perfused gently (25 mL of phosphate buffer) and brains (left hemisphere) were collected. Blood samples were centrifuged for 5 min at 4600 RPM to separate blood plasma from cells. The plasma (100 μL) was diluted in acetonitrile (200 μL at 0 °C) and centrifuged for 5 min at 15,000 RPM for removal of proteins. Brains were homogenized in acetonitrile (200 μL at 0 °C) and centrifuged for 5 min at 15,000 RPM. An aliquot of each supernatant (10 μL) was transferred to a TLC plate, which was subsequently dried at room temperature for 5 min and ran in a solution of DCM/MeOH/TEA (90:10:1, v/v/v). The radioTLC plate was transferred to a phosphorimager storage screen and left for 1 h. Readout was performed on a Typhoon phosphorimager and subsequent analysis was performed using ImageJ.

2.8. Biodistribution of [^{11}C]BLZ945

Mice (10–16 weeks old, 25–30 g, $n = 3$ per time point) were injected with [^{11}C]**BLZ945** (100 μL, approximately 10 MBq) under isoflurane anesthesia (2% in O_2 at 1 L/min). At the indicated time-points blood was collected by arterial puncture, approximately 0.5 mL) and transferred to a Heparin coated Eppendorf tube. Mice were perfused gently (25 mL of phosphate buffer) to remove the blood component from organs. Organs were collected, weighed, and counted using a gamma counter. Results are expressed as percent of injected dose per gram (% ID/g) ± standard deviation.

2.9. PET and PET/CT scanning

Mice were anesthetized with 2% isofluorane gas in O_2 at 1 L/min and catheterized in their tail vein. When indicated, cyclosporin A was administered by tail vein injection 30 min prior to the start of PET scanning at 30 mg/kg, formulated at 20 mg/mL in DMSO, EtOH, polyethylene glycol 400, and H_2O (1/15/50/34 v/v/v/v). Unlabeled BLZ945 was formulated in 10% EtOH in saline and administered by co-injection with [^{11}C]BLZ945. PLX3397 (Selleckchem) was dosed at 5 mg/kg, formulated by dissolving in the cyclosporin A solution and administered by tail vein injection 30 min prior to tracer administration. [^{11}C]BLZ945 was administered (10–15 MBq in 100 μL) by tail vein injection. After PET scanning, mice were sacrificed by cervical dislocation and brains were collected, weighed, and activity levels were determined using a gamma counter. Time-activity curves were obtained by drawing regions of interest using PMOD. Results are expressed as the average %ID/g ± standard deviation ($n = 4$ per experimental group).

2.10. Autoradiography

Autoradiography was performed in flash frozen mouse brain sections (10 μm thickness). Sections were washed with 50 mM Tris-HCl buffer (pH 7.4) for 15 min. After drying under a gentle air flow the sections were incubated with [^{11}C]**BLZ945** (0.5 MBq·mL^{-1}) in 50 mM Tris-HCl, pH 7.4 with 3% BSA in the absence or presence of a CSF-1R inhibitor at 1 μM concentration for 30 min. Washing was performed with cold Tris-HCl (5 mM, 4 °C, two times) followed by dipping in ice cold water. After drying in an air stream, mouse brain sections were exposed to a phosphorimaging screen (GE Healthcare, Buckinghamshire, UK) for 30 min and developed on a Typhoon FLA 7000 phosphor imager (GE Healthcare, Buckinghamshire, UK). Visualisation of binding was performed using ImageQuantTL v8.1.0.0 (GE Healthcare, Buckinghamshire, UK). Data are expressed as % of binding relative to [^{11}C]**BLZ945** binding in the absence of CSF-1R inhibitor ($n = 3$).

2.11. Statistical analysis

Statistical analysis was performed using a one-sided, unpaired Student's *t*-test.

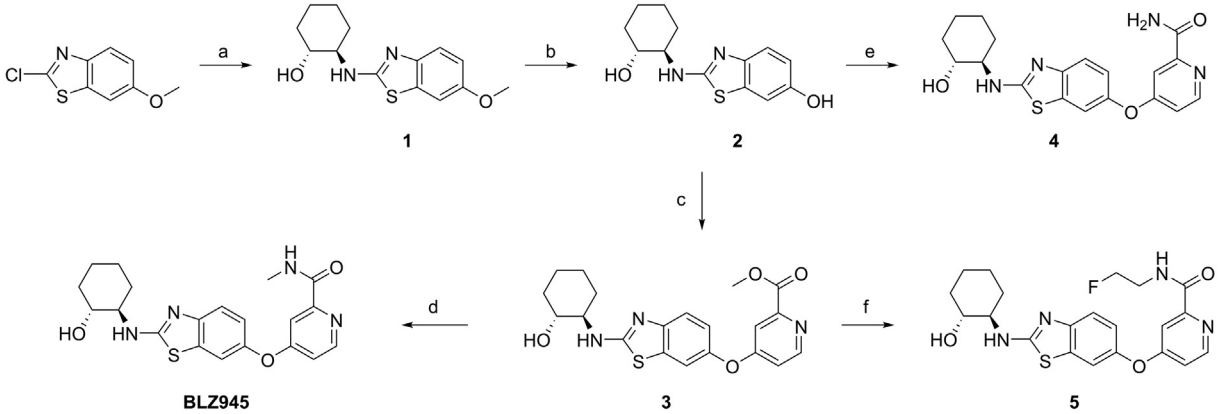

Scheme 1. Synthesis of **BLZ945**, analogue **5** and precursor **4** for carbon-11 radiolabeling. Reagents and conditions: a) (1*R*,2*R*)-2-aminocyclohexan-1-ol, TEA, NMP, 120 °C, 48 h, 59%; b) BBr_3, TEA, DCM, 0 °C to rt., 3 h, 90%; c) methyl 4-fluoropicolinate, K_2CO_3, DMF, 100 °C, 16 h, 51%; d) methylamine·HCl, K_2CO_3, THF, 50 °C, 16 h, 80%; e) 4-fluoropicolinamide, K_2CO_3, DMF, 100 °C, 16 h, 80%; f) i) KOH, MeOH/THF/H_2O, rt., 1 h; ii) 2-fluoroethylamine·HCl, HATU, DiPEA, rt., 16 h, 58%.

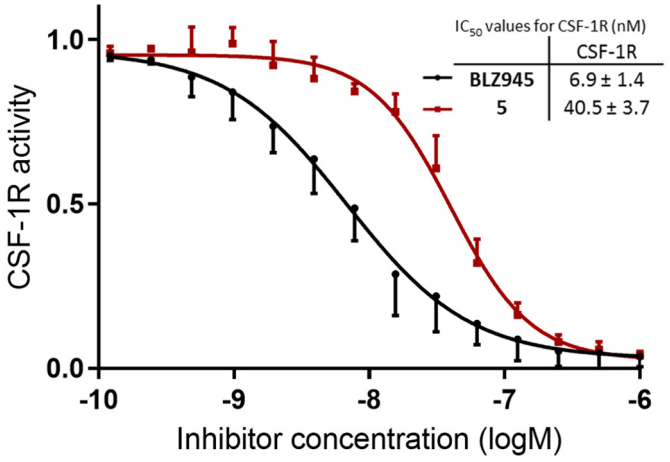

Fig. 2. Inhibition of compounds towards CSF-1R.

3. Results and discussion

3.1. Chemistry

Based on the chemical structure, direct radiolabeling of **BLZ945** at the *N*-methyl functionality with carbon-11 (Fig. 1) is feasible by reacting [^{11}C]CH_3I with the *des*-methyl precursor molecule [24]. In addition, efforts were made to design a derivative that allows for fluorine-18 labeling and thus has improved properties for PET imaging (Scheme 1) [25]. A substitution of the methyl functionality for a fluoroethyl group was envisioned to allow for potential fluorine-18 labeling [26]. The synthesis of the target compounds and their respective precursor molecules for radiolabeling was based on reported literature procedures [9,27] and is depicted in Scheme 1. Briefly, 2-chloro-6-methoxybenzothiazole was reacted with (1*R*,2*R*)-2-aminocyclohexanol to obtain benzothiazole **1**, which was then subjected to *O*-demethylation using BBr_3, affording compound **2**. Subsequent nucleophilic aromatic substitution using 4-fluoropicolinamide resulted in **BLZ945** precursor **4**. Methyl ester **3** was obtained by reaction of compound **2** with methyl 4-fluoropiconilate. Compound **3** was then converted to **BLZ945** by treatment with methylammonium chloride and to fluoro-ethyl analogue **5** by alkaline deprotection followed by HATU-mediated coupling with fluoroethylamine.

3.2. In vitro evaluation

Both **BLZ945** and analogue **5** were tested for their inhibitory potency *in vitro* against human recombinant CSF-1R (Fig. 2) using a commercially available *Z*-LYTE™ assay kit. In addition, selectivity over c-Kit and PDGFR-β, close family members of CSF-1R with high structural homology [28], was determined. **BLZ945** was found to be most potent, with IC_{50} value of 6.9 ± 1.4 nM. The fluoroethyl analogue **5** resulted in an increase in IC_{50} to 40.5 ± 3.7 nM, demonstrating the preference for a methylamide at this position. In accordance with the general selectivity for this scaffold, no inhibition of c-KIT and PDGFR-β was observed at concentration up to 4 μM [27]. As a result of this affinity and selectivity screening, **BLZ945** was selected as the optimal candidate for radiolabeling.

3.3. Radiolabeling, QC and in vitro evaluation

Carbon-11 synthesis of **BLZ945** was pursued by direct methylation of precursor amide **4**. Although this precursor has an aminocyclohexanol functionality that might benefit from protection to avoid the formation of side products, such strategy would require multi-step syntheses and the resulting elongated synthesis time might not outweigh the improved radiochemical conversion to [^{11}C]**BLZ945**. Following a one-step strategy, [^{11}C]**BLZ945** was efficiently synthesized by reacting precursor **4** with [^{11}C]CH_3I in the presence of tetrabutylammonium hydroxide (1.0 M solution in MeOH) in DMSO (Fig. 3). The main radiochemical product was [^{11}C]**BLZ945**, the identity of which was confirmed by coinjection of an authentic reference sample on HPLC using two distinct HPLC conditions (Supporting Information Fig. S1). The full synthetic procedure, from end of bombardment to formulation in 10% EtOH in saline, was performed in a fully automated fashion in 60 min and gave [^{11}C]**BLZ945** in 20.7 ± 1.1% decay corrected yield (2.58 ± 0.14 GBq at end of synthesis), a molar activity of 153 ± 34 GBq·μmol^{-1} and a radiochemical purity >95% (n = 5, Supporting Information Fig. S1).

[^{11}C]**BLZ945** remained stable in solution as well as in mouse plasma up to 1 h (Supporting information Fig. S1). The partition coefficient LogD was empirically determined as 2.26 ± 0.01 by the shake flask method. This value is comparable with the calculated LogP of 3.09 (ChemDraw Professional, v16.0.1.4) and well within the range for successful brain penetration [29].

3.4. Ex vivo evaluation

Potential metabolism of [^{11}C]**BLZ945** was determined *ex vivo* by radioTLC analysis of blood plasma and brain homogenates at 15, 30, and 60 min post injection in healthy mice (n = 3 per time point). Both in plasma and brain only, intact tracer was detected, demonstrating the excellent metabolic stability of **BLZ945** up to 1 h post injection (Supporting information Fig. S2). These findings correspond well with the reported high stability of [^{14}C]**BLZ945** in human hepatocytes and microsomes [30]. *Ex vivo* tracer distribution was determined at 15, 30, and 60 min post injection in healthy mice (Fig. 4 and Supporting Information Table S1). In accordance with its pharmaceutical activity in mouse models of glioblastoma [9], [^{11}C]**BLZ945** displayed good brain penetration of approximately 1%ID/g. Moderate washout was observed, which could potentially be attributed to the basal expression of CSF-1R on microglia in the healthy brain [31]. Blood radioactivity concentrations were relatively high, potentially due to the high plasma protein binding (96%) and low free fraction (4%) of **BLZ945** [30]. Excretion mainly occurs *via* the hepatic system, as evidenced by high radioactivity concentrations in liver and intestines and low values for kidney and urine.

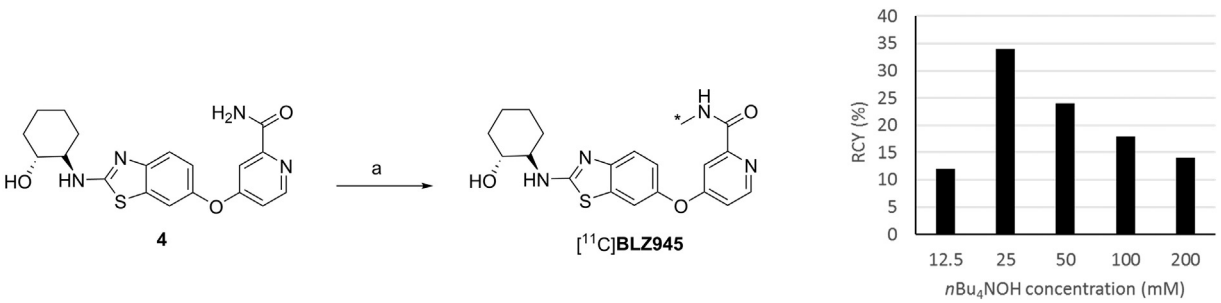

Fig. 3. Optimization of radiolabeling conditions towards [^{11}C]**BLZ945**. Reagents and conditions: a) TBAOH (1.0 M in MeOH), DMSO, 100 °C, 5 min.

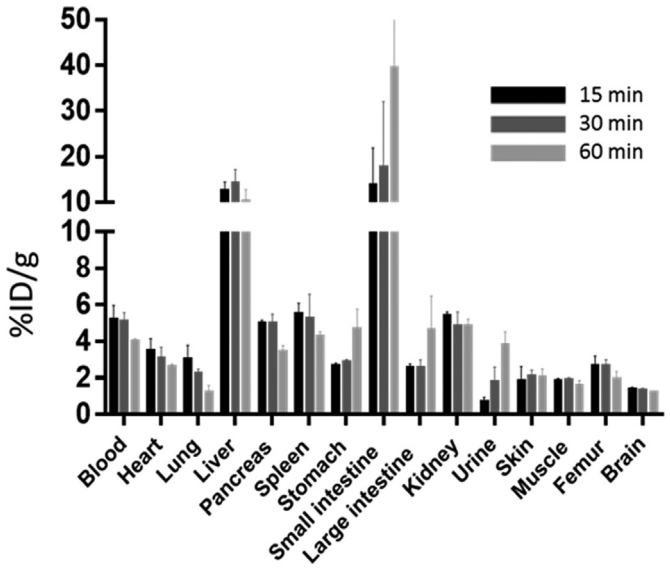

Fig. 4. *Ex vivo* tissue distribution of [^{11}C]**BLZ945** following administration to healthy mice ($n = 3$). Error bars indicate standard deviations (n = 3 per time point).

3.5. In vivo evaluation

Dynamic distribution of [^{11}C]**BLZ945** in mice brain was evaluated by means of PET scanning. Brain uptake was determined in different experimental conditions; besides administration to non-treated mice, [^{11}C]**BLZ945** was administered to mice that were pretreated with cyclosporine A (30 mg/kg, 30 min prior to PET tracer administration). Blocking experiments were performed using excess unlabeled **BLZ945** (1 mg·kg^{-1}, co-injection with radiotracer) and **PLX3397** (5 mg/kg, 30 min prior to PET tracer administration). **BLZ945** is a substrate for efflux transporters, as evidenced by the approximate 2-fold increase of brain activity levels when comparing baseline with efflux transporter inhibition at 60 min post injection ($p = 0.0003$). Specific binding of [^{11}C]**BLZ945** was demonstrated by co-administration of unlabeled **BLZ945**, which resulted in a 20% decrease in brain activity concentrations at 60 min post injection ($p = 0.05$). At time-points up to 8 min post injection, brain radioactivity levels were higher for the **BLZ945** blocking conditions, potentially due to displacement of [^{11}C]**BLZ945** in peripheral organs, resulting in increased blood concentrations. Indeed, higher blood concentrations (determined as heart TACs) were found in this blocking condition at earlier time points (Supporting information Fig. S3). The suggestion that this initial increase in brain activity level is due to increased tracer availability and not a result of CSF-1R binding is further supported by the accelerated washout of [^{11}C]**BLZ945** when compared to unblocked conditions. **PLX3397** pretreatment (i.v. administration, 5 mg/kg, 30 min prior to tracer injection), did not result in a blocking effect. **PLX3397** is designed to bind at the juxtamembrane domain of CSF-1R in the auto-inhibited state [32], which is only partially overlapping with the ATP-binding domain. The binding domain of **BLZ945** has not been reported, but based on the ATP competitive binding, it is likely that **BLZ945** directly occupies the ATP binding site. The potentially differing binding domains could explain the lack of a blocking effect of [^{11}C]**BLZ945** binding upon **PLX3397** pretreatment. Similar lack of blocking has previously been reported using CSF-1R PET tracer [^{11}C]**CPPC**. Here, no blocking effect of **PLX3397** was observed by *in vitro* autoradiography studies on human Alzheimer's disease brain sections [16], whereas **BLZ945** co-incubation did result in anticipated blocking. The brain radioactivity concentrations determined by PET imaging were confirmed by post-scanning biodistribution (Fig. 6), which overlapped very well with PET scanning results (Fig. 5B). The efflux transporter substrate behavior of **BLZ945**, which is evidenced by the increased brain uptake upon Cyclosporin A pretreatment, could potentially hamper clinical translation, as efflux transporter inhibition in human is not recommended.

3.6. Autoradiography

Finally, *in vitro* autoradiography on mouse brain sections using [^{11}C]**BLZ945** was performed. Various CSF-1R inhibitors were used for

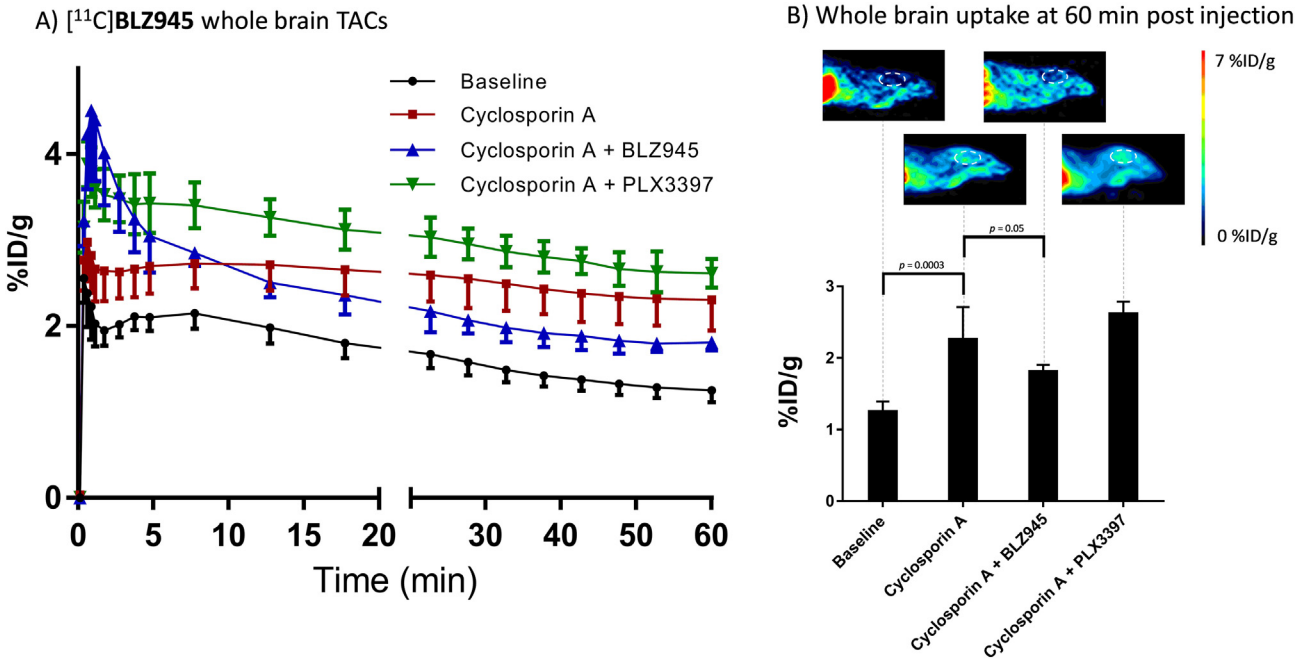

Fig. 5. *In vivo* brain uptake of [^{11}C]**BLZ945** in healthy mice. A) Time-activity-curves (TACs) of whole mouse brain at different experimental conditions; B) Brain uptake at 60 min post injection and representative coronal sections of mice from the corresponding experimental groups. Brain regions are indicated with white dotted circles. Results are expressed as average ± standard deviation ($n = 4$).

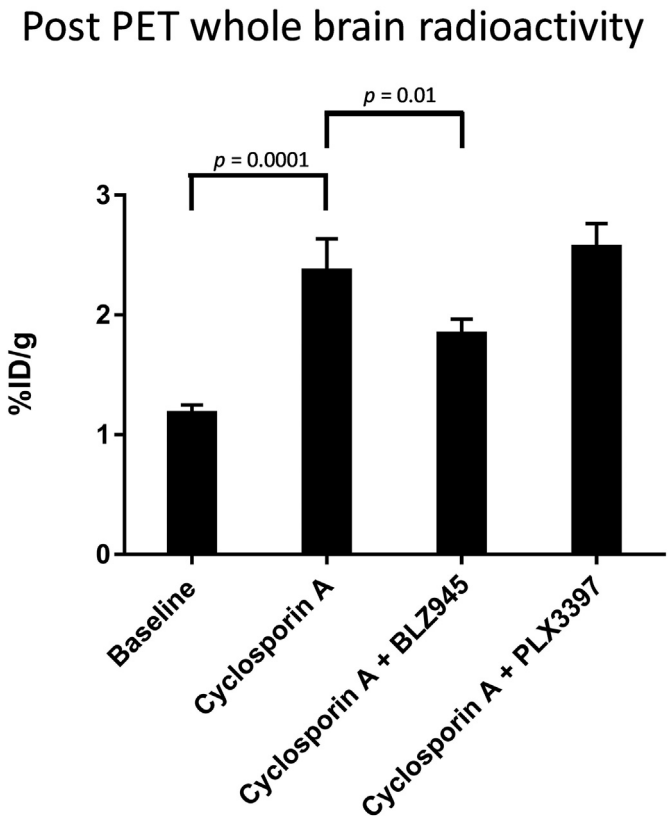

Fig. 6. Post-mortem brain activity concentrations. Results are expressed as the average ± standard deviation (n = 4 per group).

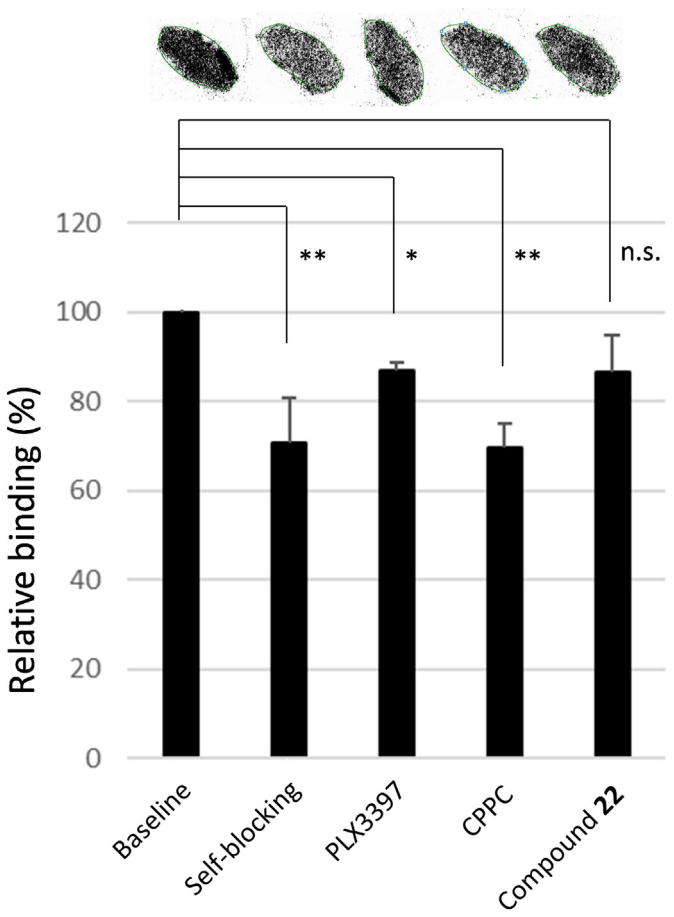

Fig. 7. *In vitro* autoradiography with [^{11}C]**BLZ945** on mouse brain sections. Representative brain slices are depicted together with quantification of binding relative to baseline conditions ([^{11}C]**BLZ945** only). CSF-1R inhibitors were used at 1 μM. (* indicates $p < 0.05$, ** indicates $p < 0.005$, n.s. not significant, $n = 3$).

blocking of [^{11}C]**BLZ945** binding (Fig. 7) [9,16,23,32].

The most pronounced blocking of [^{11}C]**BLZ945** binding was observed when using an excess of **BLZ945** or when using CPPC as a CSF-1R inhibitor. The blocking effect was about 30%, indicating specific and selective binding of [^{11}C]**BLZ945** to the brain tissue. However, this result also demonstrates that about 70% of binding is non-specific. This modest drop in binding corresponds well with PET imaging results, where a modest decrease of [^{11}C]**BLZ945** binding of approximately 20% was observed. **PLX3397** blocking showed a less pronounced blocking effect, again in close accordance with PET imaging results. Similar results were obtained using the bisamide CSF-1R inhibitor 'compound **22**'. Overall, the autoradiography results confirm the high non-specific binding observed in PET imaging experiments. This non-specific binding was observed with [^{11}C]**CPPC** as well and drastically hampers CSF-1R PET imaging [16]. Given that [^{11}C]**BLZ945** is also a strong substrate for efflux transporters, no further efforts were undertaken to evaluate the compound in animal models of CSF-1R overexpression, such as a glioblastoma model. Instead, future work will focus on identifying CSF-1R PET tracers that do not suffer from efflux transport and less from non-specific binding compared to the currently reported CSF-1R PET tracers, which is especially relevant when considering the modest increases in CSF-1R expression in various animal models [33–36]. To assist in the compound selection, the use of both *in silico* (*e.g.* CNS-MPO-PET scoring) and *in vitro* screening tools (*e.g.* lipid binding assay [37]) are recommended to optimize the tracer development process.

4. Conclusion

[^{11}C]**BLZ945**, a highly potent and selective CSF-1R inhibitor, was successfully obtained in high yield and purity. Unfortunately, because of the strong efflux transporter substrate behavior and high non-specific binding in the brain, [^{11}C]**BLZ945** seems unsuitable as a PET tracer for imaging of CSF-1R expression levels in the brain. Therefore, future work will focus on radiolabeling and evaluation of structurally distinct CSF-1R inhibitors. Further research on [^{11}C]**BLZ945** or fluorine-18 labeled derivatives could focus on imaging of accumulation of macrophages in the periphery, where efflux transport at the blood-brain-barrier is irrelevant and non-specific binding in the relevant tissue might be lower (*e.g.* cancers, inflammation or atherosclerotic plaques) [38].

Funding

The project was supported, in part, by The Ben and Catherine Ivy Foundation (FTC), the National Cancer Institute: R21 CA205564 (FTC) & T32 CA118681 (JLK), and the National Institutes of Health: S10 OD018130 (FTC).

Availability of data and materials

Please contact author for data requests.

Ethics approval and consent to participate

Not applicable.

Declaration of competing interest

There are no competing interests to report.

Acknowledgments

We thank Tim Doyle and the Stanford Small Animal Imaging Facility for their technical assistance.

Appendix A. Supplementary data

Supplementary data to this article can be found online at https://doi.org/10.1016/j.nucmedbio.2021.06.005.

References

[1] Louis DN, Perry A, Reifenberger G, von Deimling A, Figarella-Branger D, Cavenee WK, et al. The 2016 World Health Organization classification of tumors of the central nervous system: a summary. Acta Neuropathol. 2016;131:803–20.
[2] Johnson DR, O'Neill BP. Glioblastoma survival in the United States before and during the temozolomide era. J Neurooncol. 2012;107:359–64.
[3] Stupp R, Mason WP, van den Bent MJ, Weller M, Fisher B, Taphoorn MJB, et al. Radiotherapy plus concomitant and adjuvant temozolomide for glioblastoma. N Engl J Med. 2005;352:987–96.
[4] Wenger KJ, Wagner M, You SJ, Franz K, Harter PN, Burger MC, et al. Bevacizumab as a last-line treatment for glioblastoma following failure of radiotherapy, temozolomide and lomustine. Oncol Lett. 2017;14:1141–6.
[5] Diaz RJ, Ali S, Qadir MG, De La Fuente MI, Ivan ME, Komotar RJ. The role of bevacizumab in the treatment of glioblastoma. J Neurooncol. 2017;133:455–67.
[6] Chaichana KL, Zaidi H, Pendleton C, McGirt MJ, Grossman R, Weingart JD, et al. The efficacy of carmustine wafers for older patients with glioblastoma multiforme: prolonging survival. Neurol Res. 2011;33:759–64.
[7] Badie B, Schartner J. Role of microglia in glioma biology. Microsc Res Tech. 2001;54:106–13.
[8] Li R, Li H, Yan W, Yang P, Bao Z, Zhang C, et al. Genetic and clinical characteristics of primary and secondary glioblastoma is associated with differential molecular subtype distribution. Oncotarget. 2015;6:7318–24.
[9] Pyonteck SM, Akkari L, Schuhmacher AJ, Bowman RL, Sevenich L, Quail DF, et al. CSF-1R inhibition alters macrophage polarization and blocks glioma progression. Nat Med. 2013;19:1264–72.
[10] Cannarile MA, Weisser M, Jacob W, Jegg AM, Ries CH, Rüttinger D. Colony-stimulating factor 1 receptor (CSF1R) inhibitors in cancer therapy. J Immunother Cancer. 2017;5:53.
[11] Peyraud F, Cousin S, Italiano A. CSF-1R inhibitor development: current clinical status. Curr Oncol Rep. 2017;19:70.
[12] Walker DG, Tang TM, Lue LF. Studies on colony stimulating factor receptor-1 and ligands colony stimulating factor-1 and interleukin-34 in Alzheimer's disease brains and human microglia. Front Aging Neurosci. 2017;9:244.
[13] Ametamey SM, Honer M, Schubiger PA. Molecular imaging with PET. Chem Rev. 2008;108:1501–16.
[14] Bernard-Gauthier V, Schirrmacher R. 5-(4-((4-[(^{18})F]Fluorobenzyl)oxy)-3-methoxybenzyl)pyrimidine-2,4-diamine: a selective dual inhibitor for potential PET imaging of Trk/CSF-1R. Bioorg Med Chem Lett. 2014;24:4784–90.
[15] Tanzey SS, Shao X, Stauff J, Arteaga J, Sherman P, Scott PJH, et al. Synthesis and initial in vivo evaluation of [^{11}C]AZ683 - a novel PET radiotracer for colony stimulating factor 1 receptor (CSF1R). Pharmaceuticals. 2018;11:136.
[16] Horti AG, Naik R, Foss CA, Minn I, V Misheneva Y Du, Wang Y, et al. PET imaging of microglia by targeting macrophage colony-stimulating factor 1 receptor (CSF1R). PNAS. 2018;116:1686–91.
[17] Illig CR, Chen J, Wall MJ, Wilson KJ, Ballentine SK, Jonathan M, et al. Discovery of novel FMS kinase inhibitors as anti-inflammatory agents. Bioorg Med Chem Lett. 2008;18:1642–8.
[18] Conway JG, McDonald B, Parham J, Keith B, Rusnak DW, Shaw E, et al. Inhibition of colony-stimulating-factor-1 signaling *in vivo* with the orally bioavailable cFMS kinase inhibitor GW2580. Proc Natl Acad Sci U S A. 2005;102:16078–83.
[19] Genovese MC, Hsia E, Belkowski SM, Chien C, Masterson T, Thurmond RL, et al. Results from a phase IIA parallel group study of JNJ-40346527, an oral CSF-1R inhibitor, in patients with active rheumatoid arthritis despite disease-modifying anti-rheumatic drug therapy. J Rheumatol. 2015;42:1752–60.
[20] von Tresckow B, Morschhauser F, Ribrag V, Topp MS, Chien C, Seetharam S, et al. An open-label, multicenter, phase I/II study of JNJ-40346527, a CSF-1R inhibitor, in patients with relapsed or refractory hodgkin lymphoma. Clin Cancer Res. 2015;21:1843–50.
[21] Scott DA, Bell KJ, Campbell CT, Cook DJ, Dakin LA, Del Valle DJ, et al. 3-amido-4-anilinoquinolines as CSF-1R kinase inhibitors 2: optimization of the PK profile. Bioorg Med Chem Lett. 2009;19:701–5.
[22] Leukocyte complexity predicts breast cancer survival and functionally regulates response to chemotherapy. Cancer Discov. 2011 Jun;1(1):54–67. https://doi.org/10.1158/2159-8274.CD-10-0028 Epub 2011 Jun 1.
[23] Ramachandran Sreekanth A, Jadhavar Pradeep S, Miglani Sandeep K, Singh Manvendra P, Kalane Deepak P, Agarwal Anil K, et al. Design, synthesis and optimization of bis-amide derivatives as CSF1R inhibitors. Bioorg Med Chem Lett. 2017;15:2153–60.
[24] Poot AJ, van der Wildt B, Stigter-van Walsum M, Rongen M, Schuit RC, Hendrikse NH, et al. [^{11}C]Sorafenib: radiosynthesis and preclinical evaluation in tumor-bearing mice of a new TKI-PET tracer. Nucl Med Biol. 2013;40:488–97.
[25] Dollé F. Carbon-11 and fluorine-18 chemistry devoted to molecular probes for imaging the brain with positron emission tomography. J Labelled Comp Radiopharm. 2013;56:65–7.
[26] Tewson TJ. Synthesis of [^{18}F]Fluoroetanidazole: a potential new tracer for imaging hypoxia. Nucl Med Biol. 1997;24:755–60.
[27] Novartis AG, 6-O-substituted benzoxazole and benzothiazole compounds and methods of inhibiting CSF-1R signaling. WO2007121484.
[28] Robinson DR, Wu YM, Lin SF. The protein tyrosine kinase family of the human genome. Oncogene. 2000;19:5548–57.
[29] Pike VW. PET radiotracers: crossing the blood-brain barrier and surviving metabolism. Trends Pharmacol Sci. 2009;30:431–40.
[30] Krauser JA, Jin Y, Walles M, Pfaar U, Sutton J, Wiesmann M, et al. Phenotypic and metabolic investigation of a CSF-1R kinase receptor inhibitor (BLZ945) and its pharmacologically active metabolite. Xenobiotica. 2015;45:107–23.
[31] Akiyama H, Nishimura T, Kondo H, Ikeda K, Hayashi Y, McGeer PL. Expression of the receptor for macrophage colony stimulating factor by brain microglia and its upregulation in brains of patients with Alzheimer's disease and amyotrophic lateral sclerosis. Brain Res. 1994;639:171–4.
[32] Tap William D, Wainberg Zev A, Anthony Stephen P, Ibrahim Prabha N, Zhang Chao, Healey John H, et al. Structure-guided blockade of CSF1R kinase in Tenosynovial Giant-cell tumor. N Engl J Med. 2015;373:428–37.
[33] Wang Y, Berezovska O, Fedoroff S. Expression of colony stimulating factor-1 receptor (CSF-1R) by CNS neurons in mice. J Neurosci Res. 1999;57:616–32.
[34] Murphy GM, Zhao F, Yang L, Cordell B. Expression of macrophage colony stimulating factor receptor is increased in the AbetaPP(V717F) transgenic mouse model of Alzheimer's disease. Am J Pathol. 2000;157:890–5.
[35] Raivich G, Haas S, Werner A, Klein MA, Kloss C, Kreutzberg GW. Regulation of MCSF receptors on microglia in the normal and injured mouse central nervous system: a quantitative immunofluorescence study using confocal laser microscopy. J Comp Neurol. 1998;395:342–58.
[36] Luo Jian, Elwood Fiona, Britschgi Markus, Villeda Saul, Zhang Hui, Ding Zhaoqing, et al. Colony-stimulating factor 1 receptor (CSF1R) signaling in injured neurons facilitates protection and survival. J Exp Med. 2013;210:157–72.
[37] Assmus F, Seelig A, Gobbi L, Borroni E, Glaentzlin P, Fischer H. Label-free assay for the assessment of nonspecific binding of positronemission tomography tracer candidates. Eur J Pharm Sci. 2015;79:27–35.
[38] Zhao N, van der Wildt B, Shen B, Chin FT. ^{18}F-BLZ945 derivative with macrophage avidity facilitates PET imaging in inflamed atherosclerotic plaques. WMIC meeting abstract. Cardiovasc Imag from Basic Transl. 2019 (September 5).